https://doi.org/10.5194/egusphere-2026-5798
Preprint. Discussion started: 13 November 2026
© Author(s) 2026. CC BY 4.0 License.

# Effects of Entrainment Mixing on Three-Dimensional Ice-Liquid Mixing Homogeneity in Mixed-Phase Clouds and Their Microphysical Mechanisms

Xuemin Chen[1,2], Chunsong Lu[2*], Jing Yang[2], PengCheng Lin[2], Yangang Liu[3], Xiaodong Yan[1], Tao Liu[1], Yuting Deng[2], Jingjing Lv[2], Yue Zhou[4]

[1]Guizhou Mountainous Meteorological Science Research Institute, Guiyang, 550002, china
[2]China Meteorological Administration Aerosol-Cloud and Precipitation Key Laboratory and CMAWMC-NUIST Innovation Research Institute of Weather Modification, Nanjing University of Information Science and Technology, Nanjing, 210044, China
[3]Environmental and Climate Sciences Department, Brookhaven National Laboratory, Upton, NY, 5000, USA
[4]China Meteorological Administration Basin Heavy Rainfall Key Laboratory/Hubei Key Laboratory for Heavy Rain Monitoring and Warning Research, Institute of Heavy Rain, China Meteorological Administration, Wuhan, 430205, China

*Correspondence to*: Chunsong Lu (clu@nuist.edu.cn)

**Abstract.** Mixed-phase clouds significantly affect water cycle and energy budget, with ice-liquid mixing homogeneity (*E*) modulating precipitation formation. Previous studies focused on one-dimensional *E*; but, the evolutionary characteristics of three-dimensional *E* and mechanisms affected by entrainment mixing remain elusive. Therefore, sensitivity experiments with a mixed-phase direct numerical simulation model are conducted to bridge these gaps. First, one-dimensional *E* is sensitive to sampling direction, whereas three-dimensional *E* yields more stable statistics. Second, *E* decreases and exhibits scale dependence during entrainment mixing, with initial *E* and decay rate (*k*) modulated by initial conditions. For droplets, larger concentration and radius increase initial *E* but decrease *k*. For ice, higher concentration or smaller radius increases both initial *E* and *k*. For environmental factors, relative humidity of entrained air and mixing fraction of cloudy air correlate negatively with *k*, while weakly affecting initial *E*. Machine learning model results further indicate that grid resolution dominates *E*, where coarser grid yields higher *E*, followed by ice/droplet radius and concentration. Third, analysis of mechanisms reveals that droplet concentration and radius increase *E* by creating continuous liquid background, while abundant liquid supply suppresses evaporation, thereby reducing *k*. For ice, high concentration promotes uniform distribution of ice within liquid background, increasing *E* and *k*, whereas larger radius induces localized ice mass aggregation and segregation from liquid background, decreasing both. For environmental factors, abundant vapor supply suppresses evaporation, reducing *k*. Furthermore, coarser grid increases two-phase coexistence probabilities, thereby increasing *E*. These findings provide an important theoretical foundation for understanding and parameterizing *E*.

https://doi.org/10.5194/egusphere-2026-5798
Preprint. Discussion started: 13 November 2026
© Author(s) 2026. CC BY 4.0 License.

## 1 Introduction

Mixed-phase clouds are widespread and occur frequently in nature, exerting significant impacts on precipitation formation, radiative transfer, and the Earth's energy balance (Zelinka et al., 2020; Goosse et al., 2018; Taylor et al., 2019). The spatial distribution of cloud droplets and ice crystals within mixed-phase clouds significantly influences various microphysical processes, most notably the Wegener-Bergeron-Findeisen (WBF) process. During the WBF process, whereby the ambient water vapor is subsaturated with respect to liquid but supersaturated with respect to ice, ice crystals undergo depositional growth at the expense of water vapor evaporated from cloud droplets (Bergeron, 1935; Findeisen, 1938; Wegener, 1911). Previous studies have demonstrated that driven by turbulence and inhomogeneous evaporation, both cloud droplets and ice crystals are rarely randomly or homogeneously distributed; instead, they tend to segregate into pure liquid or pure ice regions, exhibiting prominent clustering characteristics (Dodson and Small Griswold, 2022; Saw et al., 2012; Yang et al., 2025; Ding et al., 2026). Meanwhile, distinct differences exist between the spatial distributions of cloud droplets and ice crystals. A homogeneous distribution promotes closer spatial proximity between droplets and ice crystals, thereby facilitating more efficient WBF rate. Conversely, under heterogeneous conditions, the spatial domains where the WBF process can actively occur are constrained, diminishing its overall efficiency and ultimately suppressing precipitation formation (Korolev and Milbrandt, 2022).

Studies have demonstrated that entrainment mixing is a critical process influencing the spatial distributions of ice crystals and cloud droplets within mixed-phase clouds (Liu et al., 2024). The entrainment of ambient dry air into the cloud modulates local microphysics via two distinct pathways. On one hand, it alters the local saturation degree, thereby driving the liquid-to-ice phase transition (Pinsky and Khain, 2018). On the other hand, the turbulent mixing and dilution affected by entrainment change the spatial inhomogeneity of the in-cloud temperature, water vapor, and particle fields. This further modifies the spatial distribution of droplets and ice crystals, and consequently impacts the occurrence of the WBF process as well as the cloud phase transition (Liu et al., 2024; Shupe et al., 2012). Therefore, to accurately understand the microphysical process in entrainment-affected mixed-phase clouds, it is imperative not only to focus on the spatial distribution characteristics of ice crystals and cloud droplets, but also to quantitatively characterize their mixing homogeneity.

Previous studies have quantified the inhomogeneity of particle phase distributions within clouds. Using the pair correlation function (PCF) approach, Kostinski and Shaw (2001) and Shaw et al. (2006) estimated the scales of cloud droplet clustering, showing that these clusters can reach centimeter-to-decimeter scales and that small-scale clustering is primarily driven by turbulence. Similarly, employing the PCF algorithm, Deng et al. (2024a) demonstrated that the characteristic scales of ice crystal cluster can span from 100 m to 3.2 km. Subsequently, they utilized an information-theoretic entropy algorithm to characterize the ice-liquid mixing homogeneity and proposed its parameterization schemes as a function of total water content and temperature (Deng et al., 2024b). Furthermore, Korolev and Milbrandt (2022) pointed out that clustering scales can extend from 100 m to 100 km, with the cluster distribution obeying a -3/5 power-law relationship. More recently, Yang et al. (2024) noted that mixed-phase cluster length is related to the glaciation process, whereby a faster glaciation process leads to a shorter

https://doi.org/10.5194/egusphere-2026-5798
Preprint. Discussion started: 13 November 2026
© Author(s) 2026. CC BY 4.0 License.

mixed-phase cluster length. Ding et al. (2026) pointed out that active secondary ice production within convective cores of shallow mixed-phase clouds promotes rapid localized glaciation, resulting in isolated ice patches.

In general, previous efforts have achieved significant progress in identifying cloud particle clustering characteristics and characterizing ice-liquid mixing homogeneity. However, relevant research has been mostly confined to the one-dimensional (1-D) scale, rarely extending to the three-dimensional (3-D) scale. The limitation arises primarily because, constrained by current observational technologies, high-resolution 3-D microphysical information remains challenging to acquire. Furthermore, the evolutionary characteristics of ice-liquid mixing homogeneity under the influence of entrainment mixing, as well as the underlying physical mechanisms remain elusive. The reason is that entrainment mixing is closely coupled with turbulence and operates at small spatial scales, making direct observations challenging (Lu et al., 2023; Liu et al., 2023). Meanwhile, most numerical models still struggle to explicitly resolve small-scale turbulent eddies. Therefore, high-resolution numerical simulations are required to bridge these critical research gaps.

The particle-resolved direct numerical simulation (PR-DNS) model is a numerical approach capable of explicitly resolving turbulence and its microphysical responses while simultaneously tracking individual particle trajectories, thereby capturing comprehensive 3-D microphysical information (Chen et al., 2025; Gao et al., 2018; Zhang et al., 2024). Since the early 21st century, DNS has been widely utilized to investigate microphysical processes in warm clouds (Andrejczuk et al., 2009; Chen et al., 2021; Kumar et al., 2018). Following continuous development and refinement, DNS has now been extended to study microphysical process in mixed-phase clouds, serving as an indispensable research tool in this field (Chen et al., 2023; Wang et al., 2024).

On this basis, to address the lack of research on 3-D ice-liquid mixing homogeneity and the unclear effects and mechanisms of entrainment on it, this study utilizes a high-resolution mixed-phase DNS model to conduct a series of sensitivity experiments and obtain high-resolution 3-D microphysical information. Combined with an information-theoretic entropy algorithm, the 3-D ice-liquid mixing homogeneity is quantitatively characterized. The differences between 1-D and 3-D ice-liquid mixing homogeneity, and underlying mechanisms affected by entrainment are explored. Finally, machine learning models (extreme gradient boosting (XGBoost) model and ensemble machine learning algorithm) coupled with Shapley Additive exPlanations (SHAP) interpretability analysis, are employed to identify the relative contributions and physical mechanisms of key microphysical variables influencing ice-liquid mixing homogeneity. This study provides a theoretical foundation for understanding ice-liquid mixing homogeneity and developing its future parameterization schemes.

## 2 Model and Methods

The mixed-phase DNS model used in this study follows the improved framework developed by Chen et al. (2026), which was designed to investigate the effects of turbulent entrainment mixing on the microphysical characteristics of mixed-phase clouds. The physical processes considered in the model includes the condensation/evaporation of cloud droplets, the deposition/sublimation of ice crystals, and the sedimentation of cloud droplets and ice crystals, whereas other processes such

https://doi.org/10.5194/egusphere-2026-5798
Preprint. Discussion started: 13 November 2026
© Author(s) 2026. CC BY 4.0 License.

as collision-coalescence and riming are excluded. Furthermore, ice crystals are assumed to be spherical. The simulation domain is configured as a cube with a length ($L$) of 0.1459 m under periodic boundary conditions, where the central region represents the cloudy area flanked by dry air areas on both sides. The grid number is set to $128^3$, and the initial turbulent dissipation rate is set to $2 \times 10^{-3}$ m$^2$ s$^{-3}$. Initially, cloud droplets and ice crystals are randomly distributed within the cloudy area. Detailed configurations of the model can be found in Chen et al. (2026).

### 2.1 Numerical Experiments

Consistent with Chen et al. (2026), the sensitivity experiments primarily focus on three aspects: liquid water content (LWC), ice water content (IWC), and environmental factors. A total of nine experiment groups is conducted, with the specific parameters summarized in Table 1. The LWC-focused experiments comprise three sets: Set 1: varying the cloud droplet number concentration ($n_d$); Set 2: varying the cloud droplet radius ($r_d$); and Set 3: varying both $n_d$ and $r_d$ simultaneously while maintaining a constant initial LWC. Similarly, the IWC-focused experiments consist of: Set 4: varying the ice crystal number concentration ($n_i$); Set 5: varying the ice crystal radius ($r_i$); Set 6: varying both $n_i$ and $r_i$ simultaneously while maintaining the initial IWC constant. The environmental factors are also investigated through three sets: Set 7: varying the relative humidity of entrained dry air ($RH_e$), Set 8: varying the mixing fraction of cloudy air ($\chi$); and Set 9: varying Taylor microscale Reynolds number ($R_e$).

A cloud sample is identified when the cloud particle number concentration $n_c$ (sum of $n_d$ and $n_i$) exceeds 10 cm$^{-3}$ and the cloud water content (CWC = LWC + IWC) is greater than 0.001 g m$^{-3}$. Based on $n_c$ and CWC, clouds can be classified into two categories of ultimate states: a cloud is defined as a mixed-phase cloud if both $n_c$ and CWC within the simulation domain remain above their respective thresholds at the end of the simulation; otherwise, it is classified as a dissipating cloud if either $n_c$ or CWC falls below these thresholds at any point during the simulation.

### 2.2 Quantification of 3-Dimensional Ice-Liquid Mixing Homogeneity

Consistent with Deng et al. (2024b), the concept of information-theoretic entropy is adopted to characterize the ice-liquid mixing homogeneity. This concept framework was originally introduced by Whittaker (1972) to quantify species diversity, and has recently been applied to investigate the inhomogeneity of aerosol distribution (Wang et al., 2023).

Assuming that the simulation domain is partitioned into $N$ grid cells (or sample units) along each of the three directions, there are a total of $N^3$ grid boxes. For each grid box, CWC, liquid mass fraction (LMF), and ice mass fraction (IMF) are denoted as $CWC_j$, $LMF_j$, and $IMF_j$ ($j$ = 1, 2, …, $N^3$), respectively, where $LMF_j + IMF_j = 1$.

$$H_\alpha = \sum_{j=1}^{N^3}(-\mathrm{LMF_j} \times ln\mathrm{LMF_j} - \mathrm{IMF_j} \times ln\mathrm{IMF_j}) \times c_j, \quad (1)$$

$$H_\gamma = -\overline{\mathrm{LMF}} \times ln\overline{\mathrm{LMF}} - \overline{\mathrm{IMF}} \times ln\overline{\mathrm{IMF}}, \quad (2)$$

$$\overline{\mathrm{LMF}} = \sum_{j=1}^{N^3} \mathrm{LMF_j} \times c_j, \quad (3)$$

https://doi.org/10.5194/egusphere-2026-5798
Preprint. Discussion started: 13 November 2026
© Author(s) 2026. CC BY 4.0 License.

$$\overline{\mathrm{IMF}} = \sum_{j=1}^{N^3} \mathrm{IMF_j} \times c_j, \quad (4)$$

$$E = \frac{e^{H_\alpha} - 1}{e^{H_\gamma} - 1} = \frac{D_\alpha - 1}{D_\gamma - 1}, \quad (5)$$

where $H_\alpha$ and $H_\gamma$ denote the mean mixing entropy and population mixing entropy, respectively; $c_j = CWC_j/CWC_{total}$, with $CWC_{total}$ representing the sum of CWC over all grid boxes; $\overline{LMF}$ and $\overline{IMF}$ denote the weighted-mean LMF and IMF, respectively; $D_\alpha$ and $D_\gamma$ represent the mean grid diversity and population diversity, respectively; and $E$ is utilized to characterize the ice-liquid mixing homogeneity, with its value ranging from 0 to 1. $E$ characterizes the degree of spatial co-location between droplets and ice crystals in mixed-phase clouds, reflecting whether the two phases are thoroughly mixed or spatially segregated into pure-phase patches. If all grid boxes contain only a pure liquid phase or ice phase, discussing the homogeneity of ice-liquid mixing is unnecessary. If each grid box consists of a pure liquid phase and a pure ice phase separately, $D_\alpha$ is low while $D_\gamma$ is high, resulting in an $E$ value of 0. Conversely, if each grid box consists of a half-liquid and half-ice, both $D_\alpha$ and $D_\gamma$ are high, resulting in an $E$ value of 1. Detailed formulations can be found in Deng et al. (2024b).

**Table 1. Parameters of the Direct Numerical Simulation (DNS) Sensitivity Experiments (Chen et al., 2026).**

| Sets number | Group | Initial conditions |
|---|---|---|
| - | Control run, CTL | Droplet concentration $n_d$ = 100 cm$^{-3}$<br>Droplet radius $r_d$ = 10 μm<br>Ice concentration $n_i$ = 100 L$^{-1}$<br>Ice radius $r_i$ = 10 μm<br>Relative humidity of entrained air $RH_e$ = 50%<br>Mixing fraction of cloudy air $\chi$ = 0.5<br>Taylor microscale Reynolds number $R_e$ = 40 |
| 1 | $n_d$ | $n_d$ = 50, 200 cm$^{-3}$ |
| 2 | $r_d$ | $r_d$ = 5, 15 μm |
| 3 | Constant liquid water content | $n_d$ = 50 and $r_d$ = 12.6, $n_d$ = 200 and $r_d$ = 7.9 |
| 4 | $n_i$ | $n_i$ = 10, 1000 L$^{-1}$ |
| 5 | $r_i$ | $r_i$ = 1, 50 μm |
| 6 | Constant ice water content | $n_i$ = 10 and $r_i$ = 17.1, $n_i$ = 1000 and $r_i$ = 4.6 |
| 7 | $RH_e$ | $RH_e$ = 20%, 80% |
| 8 | $\chi$ | $\chi$ = 0.2, 0.8 |
| 9 | $R_e$ | $R_e$ = 30, 47 |

https://doi.org/10.5194/egusphere-2026-5798
Preprint. Discussion started: 13 November 2026
© Author(s) 2026. CC BY 4.0 License.

## 3 Superiority of 3-D Ice-Liquid Mixing Homogeneity

In previous studies, *E* was mostly quantified based on 1-D aircraft observation data (Deng et al., 2024b). However, relying solely on 1-D information to characterize the spatial mixing state of the liquid and ice phases has inherent limitations. Figure 1 illustrates the probability density functions (PDFs) and statistical characteristics of 1-D and 3-D *E* for the control run when *N* is set to 8, 16, and 32. Here "1D *x* axis", "1D *y* axis", and "1D *z* axis" represent sampling along the *x*-, *y*-, and *z*-axes, respectively, for 1-D *E* calculation. When *N* equals 8, the skewness of 1-D *E* sampled along the *x*- and *y*-axes are -1.86 and -2.21, respectively, with corresponding kurtosis of 6.57 and 7.95. Their PDFs display a secondary peak region outside the primary peak ($E \sim 0.8$), exhibiting a significant negatively skewed and leptokurtic features. Although the skewness and kurtosis of 1-D *E* sampled along the *z*-axes (-1.00 and 0.44) are significantly reduced, they still differ markedly from those of 3-D *E* (-0.68 and -0.82). Concurrently, discrepancies exist in the mean and standard deviation of 1-D *E* among the three sampling directions: the mean values along the *x*-, *y*-, and *z*-axes are 0.72, 0.75, and 0.77, respectively, while the corresponding standard deviations are 0.14, 0.14, and 0.11, with the *x*-axis yielding the lowest mean and largest standard deviation. Such directional discrepancies resulting from 1-D sampling methods persist as *N* increases to 16 and 32. These results demonstrate that 1-D results are highly sensitive to the sampling direction; not only do the mean and standard deviation vary, but the shape of the distribution (e.g., skewness and kurtosis) also alters significantly due to interception of different cluster topologies. Consequently, relying solely on 1-D results from a single direction is prone to yielding biased or incomplete conclusions.

In contrast, the standard deviation of 3-D *E* across three grid resolutions ($N = 8$, 16, and 32) are consistently lower than those obtained from the corresponding 1-D directions. Its skewness and kurtosis also remain within relatively stable ranges, showing no extreme skewness or leptokurtic features as observed in the 1-D results. This indicates that 3-D calculation method can more comprehensively capture the relative positions and spatial information of ice crystals and cloud droplets across different directions, thereby mitigating directional discrepancies introduced by a single sampling path and yielding more stable and reliable statistical results.

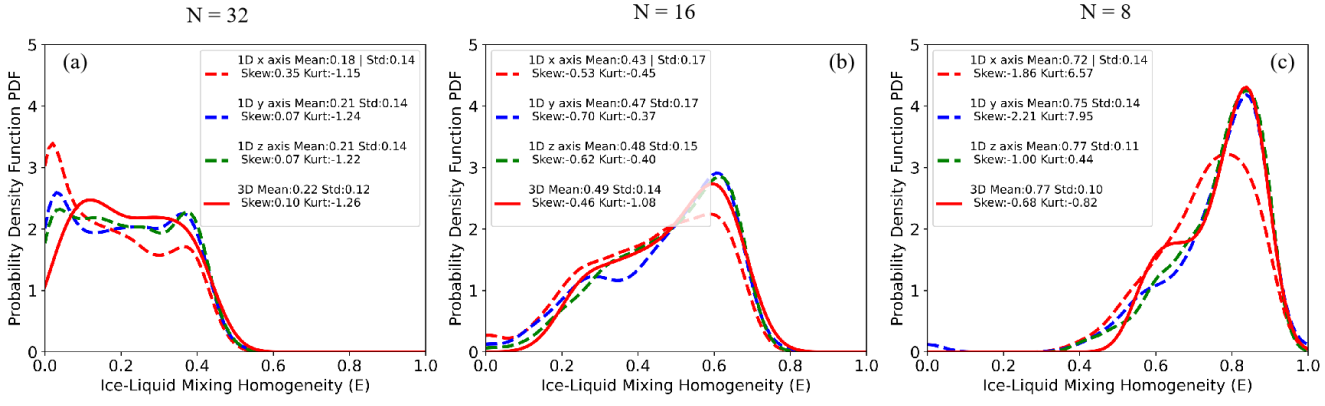



**Figure 1: Probability density functions (PDFs) of one-dimensional (1-D) and three-dimensional (3-D) ice-liquid mixing homogeneity (*E*) for the control run with number of grids (*N*) along each direction of the simulation domain set to 32, 16, and 8. In the legend, the**

https://doi.org/10.5194/egusphere-2026-5798
Preprint. Discussion started: 13 November 2026
© Author(s) 2026. CC BY 4.0 License.

**solid lines represent 3-D *E*, the dashed lines denote 1-D *E*, and different colors represent different sampling directions. "Mean", "Std", "Skew", and "Kurt" represent the mean, standard deviation, skewness, and kurtosis, respectively.**

Furthermore, the overall distribution of $E$ shifts progressively to the right as $N$ decreases, accompanied by an increase in the mean value. This trend demonstrates a distinct scale dependence of $E$: a coarse grid resolution increases the probability that cloud droplets and ice crystals are statistically grouped into the same box, thereby leading to a more homogeneous ice-liquid mixture. Based on these findings, 3-D $E$ is adopted in the subsequent analysis of this study to characterize the ice-liquid mixing homogeneity, in order to minimize the uncertainties arising from 1-D sampling directions and more completely portray the mixing state of the liquid and ice phases in 3-D scale.

## 4 Mechanisms of Entrainment Mixing effects on 3-Dimensional Ice-Liquid Mixing Homogeneity

The above results indicate that the PDF shape of $E$ is significantly influenced by spatial resolution. To further explore the underlying mechanisms of the spatial resolution effect, Figure 2 illustrates the temporal evolution of $E$ for the control run with $N$ set to 8, 16, and 32, which correspond to grid resolutions ($\Delta x$) of 18.24, 9.12, and 4.56 mm, respectively. The results show that the cloud progressively dissipates in approximately 30 s, and the $E$ values across all three $\Delta x$ cases exhibit a continuous declining trend during entrainment mixing. This indicates that the spatial distribution of ice crystals and cloud droplets evolves toward a more heterogeneous state. Concurrently, significant discrepancies are observed in both the magnitude and decay rate of $E$ across different $\Delta x$ cases, which is consistent with the prior conclusion regarding the scale dependence of $E$. Specifically, a coarser grid resolution yields a higher $E$ and a relatively slower decay rate, since within larger grid boxes, cloud droplets and ice crystals are more likely to be statistically grouped into the same grid box, thereby rendering the ice-liquid state more homogeneous. In contrast, under finer grid resolution conditions, $E$ values are lower and decay more rapidly, indicating that the heterogeneous distribution of the liquid and ice phases can be more fully resolved as the spatial scale decreases. Since the high spatial resolution at $N = 32$ is more favorable for identifying the impacts of entrainment and phase change processes on $E$, the subsequent analyses are performed using the results obtained at $N = 32$.

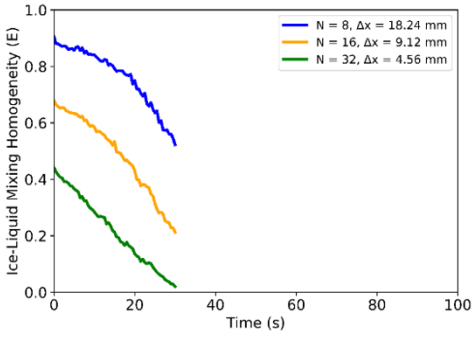



**Figure 2: Temporal evolution of ice-liquid mixing homogeneity (*E*) for the control run under different grid resolutions ($\Delta x$). In the legend, *N* represents the number of grid boxes along each direction of the simulation domain.**

https://doi.org/10.5194/egusphere-2026-5798
Preprint. Discussion started: 13 November 2026
© Author(s) 2026. CC BY 4.0 License.

Figure 3 illustrates the temporal evolution of $E$ for all sensitivity experiments listed in Table 1 when $N$ is set to 32. The continuous decline of $E$ during entrainment mixing indicates a progressive spatial segregation of the ice and liquid phases, suggesting that the entrainment mixing facilitates the formation of cluster structures. Results from different sensitivity experiments further demonstrate that the initial $E$ is significantly influenced by the initial microphysical conditions.

For LWC-focused experiments (Sets 1 and 2), the initial $E$ is positively correlated with $n_d$ and $r_d$, whereas for IWC-focused experiments (Sets 4, 5 and 6), the initial $E$ is positively correlated with $n_i$ but negatively correlated with $r_i$. Under conditions where adiabatic LWC remains constant, $RH_e$, $\chi$, and $R_e$ on the initial $E$ are relatively weak (Sets 3, 7, 8 and 9). This difference is likely attributed to the relative abundance of cloud droplets and ice crystals in the simulation domain. At the initial state, $n_d$ is approximately three orders of magnitude higher than $n_i$, resulting in a nearly continuous distribution of cloud droplets across the grid boxes, whereas ice crystals are more sparsely distributed. For LWC-focused experiments (Sets 1 and 2), when $n_d$ and/or $r_d$ increase, the local spatial coverage and LWC contribution of cloud droplets are enhanced, creating a more continuous and stable liquid background. Consequently, ice crystals tend to be more dispersedly embedded within the droplet population, thereby promoting two phases co-existence and leading to an increase in $E$.

For IWC-focused experiments (Sets 4, 5 and 6), as $n_i$ increases, ice crystals can distribute over a wider range of the liquid-phase environment, reducing pure liquid-phase regions and enhancing ice-liquid mixing, which subsequently increase in $E$. Conversely, when $r_i$ increases while $n_i$ remains unchanged, the newly added IWC concentrates the localized mass increment within the pre-existing ice-containing grid boxes, causing a rapid increase in the IMF of these grid boxes. Meanwhile, the vast majority of grid boxes remain purely liquid, forcing the liquid and ice phases to segregate into pure-phase clusters, which in turn reduces $E$. In contrast, for environment-focused experiments (Sets 7, 8 and 9), variations in $RH_e$, $\chi$, and $R_e$ do not alter the adiabatic number concentrations and radii of cloud droplets and ice crystals, leaving the initial $E$ unchanged.

Furthermore, the decay rate of $E$ is significantly influenced by the initial microphysical conditions. To quantitatively evaluate the decay rate, the absolute value of the time slope ($k$) of the difference in $E$ between the initial and final moments, is introduced. The specific values of $k$ for all sensitivity experiments listed in Table 1 are detailed in Table 2. The $k$ value for the control run is 0.0141 $s^{-1}$.

For LWC-focused experiments (Sets 1 and 2), $k$ decreases with increasing $n_d$ and $r_d$. The reason is that an abundant LWC supply enables the system to rapidly recover to saturation following partial droplet evaporation, thereby suppressing sustained droplet evaporation and consequently reducing $k$. The phenomenon opposes the effects of $n_d$ and $r_d$ on the initial $E$.

For IWC-focused experiments (Sets 4, 5 and 6), $k$ is positively correlated with $n_i$ but negatively correlated with $r_i$, which is related to and consistent with their effects on the initial $E$. In both $n_i$ and $r_i$ experiments, the cloud lifetime remains nearly identical and the final $E$ approaches 0 (Fig. 3); thus, by definition, $k$ correlates positively with the initial $E$. An increase in $n_i$ promotes a more homogenous distribution of ice crystals within the liquid background, thereby increasing the initial $E$ and $k$. In contrast, an increase in $r_i$ causes ice crystal mass to aggregate locally, separating it from the liquid background and thus lowering the initial $E$ and $k$. When IWC is held constant while $n_i$ and $r_i$ vary simultaneously, the variation in $k$ remains consistent with the conclusions of the two aforementioned scenarios.

https://doi.org/10.5194/egusphere-2026-5798
Preprint. Discussion started: 13 November 2026
© Author(s) 2026. CC BY 4.0 License.

For environment-focused experiments (Sets 7 and 8), $k$ decreases with increasing $RH_e$ and $\chi$, inconsistent with their effects on the initial $E$, since an abundant supply of water vapor suppresses droplet evaporation, thereby reducing $k$. Furthermore, under conditions where $R_e$ and initial LWC remain constant while $n_d$ and $r_d$ vary simultaneously, $k$ shows almost no change.

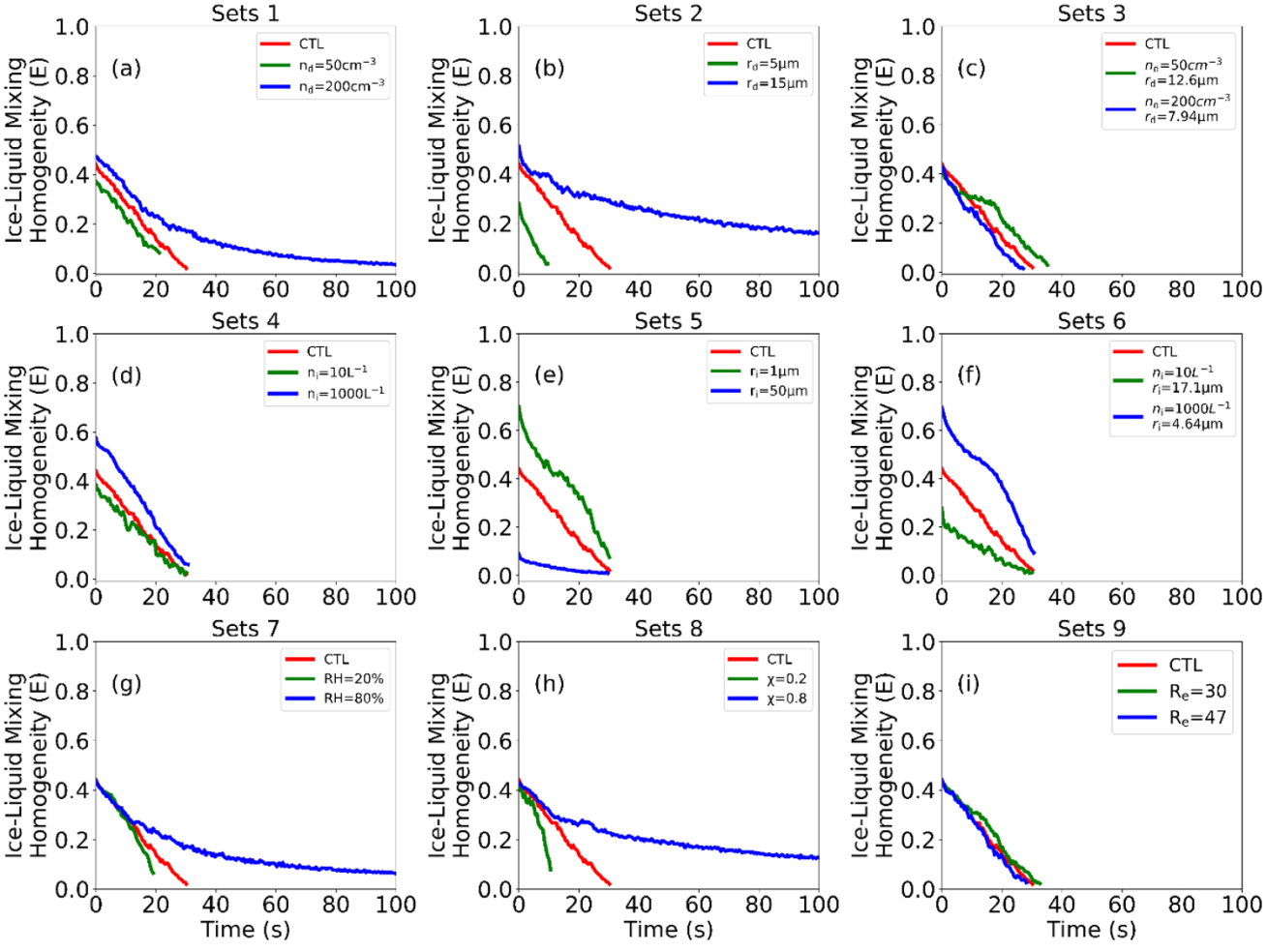



**Figure 3: Temporal evolution of ice-liquid mixing homogeneity (*E*) of all sensitivity experiments listed in Table 1.**

https://doi.org/10.5194/egusphere-2026-5798
Preprint. Discussion started: 13 November 2026
© Author(s) 2026. CC BY 4.0 License.

**Table 2. The decay rate of ice-liquid mixing homogeneity ($k$) with time for all sensitivity experiments.**

| Sets Number | Initial Conditions | Values | $k$ |
|---|---|---|---|
| - | Control run, CTL | - | 0.0141 |
| 1 | Droplet concentration, | 50 | 0.0146 |
| | $n_d$ (cm$^{-3}$) | 200 | 0.0036 |
| 2 | Droplet radius, $r_d$ (μm) | 5 | 0.0245 |
| | | 15 | 0.0026 |
| 3 | Constant initial liquid water content | $n_d$ = 50 and $r_d$ = 12.6 | 0.0104 |
| | | $n_d$ = 200 and $r_d$ = 7.9 | 0.0151 |
| 4 | Ice concentration, $n_i$ (L$^{-1}$) | 10 | 0.0120 |
| | | 1000 | 0.0178 |
| 5 | Ice radius, $r_i$ (μm) | 1 | 0.0171 |
| | | 50 | 0.0020 |
| 6 | Constant initial ice water content | $n_i$ = 10 and $r_i$ = 17.1 | 0.0073 |
| | | $n_i$ = 1000 and $r_i$ = 4.6 | 0.0171 |
| 7 | Relative humidity of entrained air, RH$_e$ (%) | 20 | 0.0189 |
| | | 80 | 0.0029 |
| 8 | Mixing fraction of cloudy air, $\chi$ | 0.2 | 0.0296 |
| | | 0.8 | 0.0024 |
| 9 | Taylor microscale Reynolds number, $R_e$ | 30 | 0.0133 |
| | | 47 | 0.0153 |

## 5 Machine Learning-Based Modeling and Analysis of the Underlying Mechanisms

The above results demonstrate that $E$ is jointly influenced by multiple microphysical conditions and exhibits a distinct scale dependence. However, the relative contributions of different microphysical variables and $\Delta x$, as well as their underlying mechanisms, require further elucidation. Therefore, the extreme gradient boosting (XGBoost) model, an ensemble machine learning algorithm, coupled with Shapley Additive exPlanations (SHAP) interpretability analysis is employed to quantify the contributions and interactions of various microphysical variables. Based on the gradient boosting framework, the XGBoost model iteratively optimizes the loss function and incorporates regularization terms, enabling it to effectively capture nonlinear responses triggered by minor parameter perturbations and complex interactions among variables (Chen and Guestrin, 2016; Friedman, 2001).

https://doi.org/10.5194/egusphere-2026-5798
Preprint. Discussion started: 13 November 2026
© Author(s) 2026. CC BY 4.0 License.

Prior to constructing the XGBoost model, the relationships between $E$ and various variables are first explored, revealing a positive correlation between $E$ and $\log_{10}$(CWC), which is consistent with the findings of Deng et al. (2024b). To more clearly characterize the relative contributions and scale features of cloud droplets and ice crystals contained within the instantaneous CWC, CWC is further decomposed into four microphysical variables: $n_d$, $n_i$, cloud droplet volume-mean radius ($r_{d,v}$), and ice crystal volume-mean radius ($r_{i,v}$). These variables as well as $\Delta x$ are utilized as input features for the XGBoost model in the subsequent factor analysis. During the model training process, a total of 4419 data samples is utilized. The dataset is partitioned into a development set and a testing set at a ratio of approximately 9:1, with data from the same simulation case strictly assigned to only one of the sets to prevent data leakage.

Figure 4 represents the prediction performance and interpretability analysis results of the XGBoost model constructed using $\Delta x$, $n_d$, $n_i$, $r_{d,v}$, and $r_{i,v}$ as predictors for $E$. The results demonstrate that the predicted values are highly consistent with the DNS values, yielding a determination coefficient of approximately 0.9771 and a root-mean-square error of approximately 0.0383, indicating that the model can accurately reproduce the variation characteristics of $E$ under different $\Delta x$. Samples under different $\Delta x$ exhibit distinct zoning characteristics in the scatter plot: the low-$E$ region primarily corresponds to smaller $\Delta x$ values, whereas the high-$E$ region is dominated by larger $\Delta x$ values. The result is consistent with the prior finding regarding the scale dependence of $E$.

The SHAP feature importance results further reveal that $\Delta x$ is the primary factor influencing $E$, with its mean absolute SHAP value (|SHAP|) reaching 0.1855, which is significantly higher than those of other microphysical variables (Fig. 4c). The result indicates that the scale effect exerts a stronger control on $E$ than other variables. Figure 4b shows that larger $\Delta x$ values correspond to positive SHAP, while smaller $\Delta x$ values correspond to negative SHAP, suggesting that an increase in $\Delta x$ enhances $E$. Among the microphysical variables, $r_{d,v}$ and $r_{i,v}$ are relatively important factors, with mean |SHAP| of 0.0784 and 0.0665, respectively, which are notably higher than those of $n_d$ and $n_i$. Specifically, larger $r_{i,v}$ corresponds to negative SHAP, demonstrating that an increase in ice crystal radius tends to reduce $E$, since ice crystal mass localized aggregates, causing the liquid and ice phases to segregate into pure-phase clusters. Conversely, larger $r_{d,v}$ corresponds to positive SHAP, indicating that larger cloud droplets facilitate an increase in $E$, as LWC contribution increases, promoting more homogeneous mixing. In contrast, the contributions of $n_d$ and $n_i$ are relatively weak, with mean |SHAP| of 0.0143 and 0.0187, respectively, indicating that the cloud particle number concentrations primarily play an auxiliary modulating role. Since larger $n_d$ and $n_i$ values both correspond to positive SHAP, an increase in cloud particle number concentrations promotes $E$ by enhancing the probability of ice-liquid coexistence.

To further explore whether the variations in $E$ are primarily controlled by the main effects of individual microphysical variables or modulated by their high-order nonlinear interactions, Figure 4d shows the feature attribution heatmap of SHAP interaction values for each microphysical variable derived from the TreeSHAP algorithm. A comparison of their relative magnitudes reveals that the main effects if individual variables are generally stronger than the interaction effects among them, with $\Delta x$ exhibiting the prominent main effect. In contrast, the interaction effects between any two variables are consistently weak, with a maximum value of only 0.0086, which is orders of magnitude smaller than the main effects of the individual variables. This

https://doi.org/10.5194/egusphere-2026-5798
Preprint. Discussion started: 13 November 2026
© Author(s) 2026. CC BY 4.0 License.

indicates that individual main effects overwhelmingly dominate the variations of $E$ within the current modeling framework. Notably, the main effects and interaction values of a given variable do not possess a simple arithmetic correspondence with its mean |SHAP| value, as a fundamental difference exists in their underlying computational logic. Therefore, the interaction strength results are primarily intended for judging the relative magnitude of interactions among variables, and should not be directly equated to or compared with the mean |SHAP|.

In summary, the variation in $E$ is primarily manifested as a significant scale dependence, followed by the modulating effects of microphysical variables, such as cloud particle size and number concentration within the current datasets and model framework.

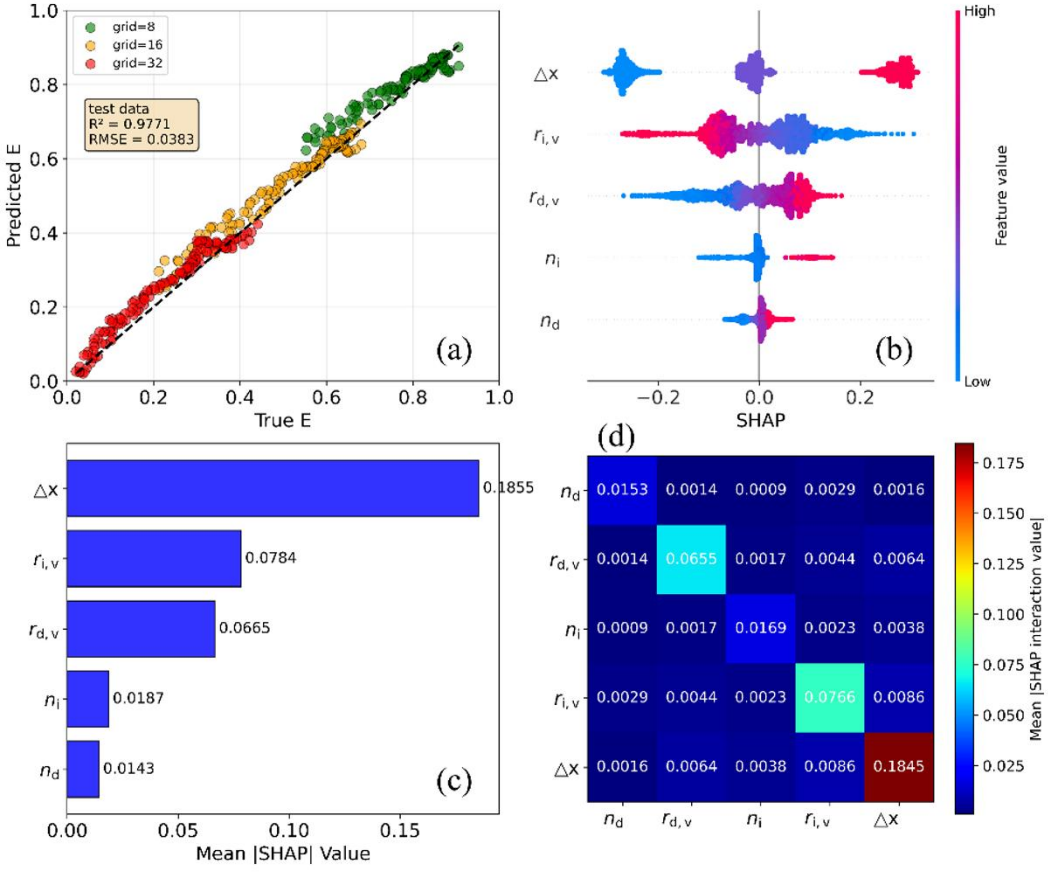



**Figure 4: (a) Prediction performance, (b) Shapley Additive exPlanations values (SHAP), (c) feature importance ranking, and (d) interaction strength heatmap of the extreme gradient boosting model for ice-liquid mixing homogeneity ($E$) under three spatial resolution ($\Delta x$) conditions. In the legend, $n_d$, $n_i$, $r_{d,v}$, and $r_{i,v}$ denote the number concentrations and volume-mean radii of cloud droplets and ice crystals, respectively; $R^2$ is the determinate coefficient; RMSE is the root-mean-square error; and "grid" represents the number of grid boxes along a single direction of the simulation domain, which can be expressed as the ratio of the domain length to $\Delta x$.**

https://doi.org/10.5194/egusphere-2026-5798
Preprint. Discussion started: 13 November 2026
© Author(s) 2026. CC BY 4.0 License.

## 6 Conclusions and Discussions

The ice-liquid mixing homogeneity ($E$) significantly influences the lifetime and radiative properties of clouds. However, current studies focus on one-dimensional (1-D) scale, with rare extensions to three-dimensional (3-D) scale, and the underlying mechanisms by which entrainment mixing affects $E$ remains elusive. Therefore, a series of sensitivity experiments using a high-resolution mixed-phase direct numerical simulation model are conducted to address this issue. Combined with an information-theoretic entropy algorithm, the 3-D $E$ is quantitatively characterized, the discrepancies between 1-D and 3-D $E$ are compared, and the impacts of entrainment mixing on $E$ as well as their physical mechanisms are investigated. On this basis, an extreme gradient boosting model coupled with Shapley Additive explanations interpretability analysis is employed to explore the relative contributions and interaction modes of relevant microphysical variables to $E$. The major conclusions are summarized as follows.

First, the probability density functions of 1-D $E$ obtained from different sampling directions exhibit significant discrepancies, indicating that 1-D $E$ is highly sensitive to the sampling direction. It is prone to introducing sampling artifacts due to the different ice-liquid phase combinations and cluster structures intercepted along different sampling directions. In contrast, 3-D $E$ can more comprehensively capture the spatial distributions and localized coexistence of ice crystals and cloud droplets within a 3-D grid without depending on a specific sampling direction. Consequently, it minimizes the uncertainties arising from single-direction sampling, making it far better suited for characterizing the actual spatial organization of the liquid and ice phases in mixed-phase clouds.

Second, the temporal evolution characteristics of 3-D $E$ during entrainment mixing are investigated. $E$ exhibits a declining trend and distinct scale dependence during entrainment mixing. Its values and decay rate ($k$) are significantly modulated by the initial conditions, where $k$ is quantified by the absolute value of the time slope of the difference between initial and final $E$. For LWC-focused experiments, initial $E$ correlates positively with droplet number concentration and radius, whereas $k$ correlates negatively with both. For IWC-focused experiments, both initial $E$ and $k$ are positively correlated with ice crystal number concentration and negatively correlated with ice crystal radius. For environment-focused experiments, the relative humidity of entrained air and mixing fraction of cloudy air have no significant effect on the initial $E$, but are negatively correlated with $k$. In experiments where LWC remains constant while droplet number concentration and radius vary and Taylor microscale Reynolds number, both the initial $E$ and $k$ show no significant changes. Additionally, analysis based on the extreme gradient boosting model indicates that grid resolution is the primary factor influencing $E$, where coarser grid yields higher $E$, followed by ice crystal and cloud droplet radii and number concentrations.

Third, the underlying mechanisms of the above findings are explored. For LWC-focused experiments, increases in cloud droplet number concentration or radius enhance liquid-phase coverage and LWC contribution, forming a continuous liquid background that embeds ice crystals more dispersedly within cloud droplet population, thereby increasing $E$. However, an abundant LWC supply enables system to rapidly recover saturation following partial evaporation, suppressing continuous evaporation and decreasing $k$. For IWC-focused experiments, higher ice crystal number concentration promotes a more

https://doi.org/10.5194/egusphere-2026-5798
Preprint. Discussion started: 13 November 2026
© Author(s) 2026. CC BY 4.0 License.

uniform distribution of ice crystals within liquid background, thereby increasing $E$. Conversely, larger ice crystal radius induces localized aggregation of ice mass and its segregation from liquid phase, leading to a decrease in $E$. Given that cloud lifetimes remain nearly identical and final $E$ approach 0 across this group experiments, $k$ is positively correlated with initial $E$, yielding consistent responses. For environment-focused experiments, higher relative humidity of entrained air and mixing fraction of cloudy air provide abundant water vapor supply, suppressing further droplet evaporation and consequently reducing $k$. Furthermore, lower grid resolution increases the probability of cloud droplets and ice crystals coexisting with the same grid, thereby increasing $E$.

This study quantitatively characterizes 3-D $E$, compares the discrepancies between 1-D and 3-D $E$, and investigates the underlying mechanisms by which entrainment mixing affects $E$. These findings provide a theoretical foundation for understanding $E$ and for constructing its parameterization schemes in the future. Note that $E$ depends on how the model domain is divided into grid cells and on the droplets and ice mass in each cell, rather than representing a cloud property that is independent of scale, and the $E$ values in this study are generally lower than the results obtained from aircraft observational data (Deng et al., 2024b; Yang et al., 2025), a difference that arises likely from the effects of sampling direction and spatial resolution. Aircraft observations obtain cloud microphysical properties along 1-D transects, whereas DNS explicitly resolves 3-D mixing characteristics of the ice and liquid phases. Furthermore, the high resolution of DNS enables the capture of finer microphysical features; in contrast, 1-D sampling may omit localized physical gradients, thereby introducing biases into the estimation of $E$. Considering that remote sensing observation instruments such as satellites and radars can acquire 2-D images, vertical profiles, and other data, future research can utilize remote sensing observation data and their retrieval products to validate model results. Nevertheless, several limitations in the current simulation setup should be acknowledged. For example, processes such as collision-coalescence and riming are excluded from the model. These processes can alter cloud particle number concentration, radius, and spatial distribution, which may in turn affect $E$. Future work will focus on improving the model by incorporating more comprehensive microphysical processes. Furthermore, enlarging the computational domain size represents another direction for future work, which help narrow the gap between DNS simulations and observations, thereby providing a basis for future microphysical parameterization applications.

## Code and data availability

The simulation data used in this study can be obtained from the Zenodo repository at https://doi.org/10.5281/zenodo.17196773 (Chen 2025).

## Author contributions

Xuemin Chen and Chunsong Lu conceived the study. Chunsong Lu designed and supervised the research. Xuemin Chen performed numerical simulations, analyzed the data, and wrote the manuscript. Jing Yang and Yangang Liu guided and

https://doi.org/10.5194/egusphere-2026-5798
Preprint. Discussion started: 13 November 2026
© Author(s) 2026. CC BY 4.0 License.

participated in the analysis. Pengcheng Lin, Xiaodong Yan, Tao Liu, Yuting Deng, Jingjing Lv, and Yue Zhou analyzed and discussed the results together.

**Competing interests**

The contact author has declared that none of the authors has any competing interests.

**Disclaimer**

Publisher's note: Copernicus Publications remains neutral with regard to jurisdictional claims made in the text, published maps, institutional affiliations, or any other geographical representation in this paper. The authors bear the ultimate responsibility for providing appropriate place names. Views expressed in the text are those of the authors and do not necessarily reflect the views of the publisher.

**Acknowledgements**

We acknowledge the High Performance Computing Center of Nanjing University of Information Science & Technology for their support of this work.

**Financial support**

The research is supported by the National Natural Science Foundation of China (42325503). Guizhou Provincial Meteorological Bureau's Open Competition Project for Selecting the Best Candidates to Lead Research (2024-N67). The appointment of Chunsong Lu at Nanjing University of Information Science & Technology is partially supported by the Jiangsu Specially-Appointed Professor (Grant R2024T01).

**References**

Andrejczuk, M., Grabowski, W. W., Malinowski, S. P., and Smolarkiewicz, P. K.: Numerical Simulation of Cloud–Clear Air Interfacial Mixing: Homogeneous versus Inhomogeneous Mixing, J. Atmos. Sci., 66, 2493-2500, 10.1175/2009jas2956.1, 2009.

Bergeron, T.: On the physics of clouds and precipitation, Proc. Fifth Assembly, 156-180, 1935.

Chen, S., Xue, L., and Yau, M. K.: Hygroscopic Seeding Effects of Giant Aerosol Particles Simulated by the Lagrangian-Particle-Based Direct Numerical Simulation, Geophysical Research Letters, 48, 10.1029/2021gl094621, 2021.

https://doi.org/10.5194/egusphere-2026-5798
Preprint. Discussion started: 13 November 2026
© Author(s) 2026. CC BY 4.0 License.



Chen, S., Xue, L., Tessendorf, S., Ikeda, K., Weeks, C., Rasmussen, R., Kunkel, M., Blestrud, D., Parkinson, S., Meadows, M., and Dawson, N.: Mixed-phase direct numerical simulation: ice growth in cloud-top generating cells, Atmospheric Chemistry and Physics, 23, 5217-5231, 10.5194/acp-23-5217-2023, 2023.

Chen, T. and Guestrin, C.: Xgboost: A scalable tree boosting system, 785-794, 2016.

Chen, X., Lu, C., Liu, Y., Chen, S., Wang, L.-P., and Yang, J.: Entrainment Mixing Modulates the Wegener–Bergeron–Findeisen Process in Mixed-Phase Clouds: Insights from Direct Numerical Simulation, J. Atmos. Sci., 83, 2039-2052, 10.1175/JAS-D-25-0195.1, 2026.

Chen, X.: Entrainment Mixing Modulates the Wegener-Bergeron-Findeisen Process in Mixed-Phase Clouds: Insights from Direct Numerical Simulation, Zenodo [dataset], https://doi.org/10.5281/zenodo.17196773.

Chen, X., Luo, S., Liu, Y., Chen, J., Zhang, T., and Lu, C.: Convergence of Cloud Droplet Spectral Relative Dispersion During Entrainment-Mixing Based on Particle-Resolved Direct Numerical Simulations, J. Geophys. Res., 130, e2025JD044265, 10.1029/2025jd044265, 2025.

Deng, Y., Yang, J., Yin, Y., Cui, S., Zhang, B., Bao, X., Chen, B., Li, J., Gao, W., and Jing, X.: Quantifying the spatial inhomogeneity of ice concentration in mixed-phase stratiform cloud using airborne observation, Atmospheric Research, 298, 10.1016/j.atmosres.2023.107153, 2024a.

Deng, Y., Yang, J., Yin, Y., Lu, C., Chen, B., Dong, X., Wang, Z., Zhang, B., Bao, X., and Hou, T.: On the Relationship Between Condensed Water Content and Liquid-Ice Mixing Homogeneity in Mixed-Phase Stratiform Clouds, Geophysical Research Letters, 51, 10.1029/2024gl110670, 2024b.

Ding, S., Liu, J. W., McFarquhar, G. M., and Gao, S.: Observations of Mixed-Phase Stratiform and Convective Cloud Regimes Over the Southern Ocean: A Case Study Near the Antarctic Polar Front, J. Geophys. Res., 131, 10.1029/2025jd043931, 2026.

Dodson, D. S. and Small Griswold, J. D.: Analyzing cloud droplet spatial tendencies on the millimetre and centimetre scales in stratocumulus clouds, Quarterly Journal of the Royal Meteorological Society, 148, 1208-1222, 2022.

Findeisen, W.: Kolloid-meteorologische vorgänge bei niederschlagsbildung, Meteor. Z, 55, 121, 1938.

Friedman, J. H.: Greedy function approximation: a gradient boosting machine, Annals of statistics, 1189-1232, 2001.

Gao, Z., Liu, Y., Li, X., and Lu, C.: Investigation of Turbulent Entrainment-Mixing Processes With a New Particle-Resolved Direct Numerical Simulation Model, J. Geophys. Res., 123, 2194-2214, 10.1002/2017jd027507, 2018.

Goosse, H., Kay, J. E., Armour, K. C., Bodas-Salcedo, A., Chepfer, H., Docquier, D., Jonko, A., Kushner, P. J., Lecomte, O., and Massonnet, F. J. N. c.: Quantifying climate feedbacks in polar regions, 9, 1919, 2018.

Korolev, A. and Milbrandt, J.: How Are Mixed-Phase Clouds Mixed?, Geophys Res Lett, 49, e2022GL099578, 10.1029/2022GL099578, 2022.

Kostinski, A. B. and Shaw, R. A.: Scale-dependent droplet clustering in turbulent clouds, Journal of Fluid Mechanics, 434, 389-398, 10.1017/s0022112001004001, 2001.

https://doi.org/10.5194/egusphere-2026-5798
Preprint. Discussion started: 13 November 2026
© Author(s) 2026. CC BY 4.0 License.

Kumar, B., Götzfried, P., Suresh, N., Schumacher, J., and Shaw, R. A.: Scale Dependence of Cloud Microphysical Response to Turbulent Entrainment and Mixing, Journal of Advances in Modeling Earth Systems, 10, 2777-2785, 10.1029/2018ms001487, 2018.

Liu, Y., Yau, M.-K., Shima, S.-i., Lu, C., and Chen, S.: Parameterization and Explicit Modeling of Cloud Microphysics: Approaches, Challenges, and Future Directions, Advances in Atmospheric Sciences, 40, 747-790, 10.1007/s00376-022-2077-3, 2023.

Liu, Y., Yang, J., Zhao, G., Deng, Y., Lu, C., Yin, Y., Jing, X., and Wang, Y.: On the Scale of Particle Clustering Induced by Inhomogeneous Entrainment-Mixing in Mixed-Phase Cumulus Clouds, Geophysical Research Letters, 51, 10.1029/2023gl107645, 2024.

Lu, C., Liu, Y., Xu, X., Gao, S., and Sun, C.: Entrainment, Mixing, and Their Microphysical Influences, in: Fast Processes in Large-Scale Atmospheric Models, Geophysical Monograph Series, 87-120, 10.1002/9781119529019.ch4, 2023.

Pinsky, M. and Khain, A.: Theoretical analysis of mixing in liquid clouds – Part IV: DSD evolution and mixing diagrams, Atmospheric Chemistry and Physics, 18, 3659-3676, 10.5194/acp-18-3659-2018, 2018.

Saw, E.-W., Shaw, R. A., Salazar, J. P. L. C., and Collins, L. R.: Spatial clustering of polydisperse inertial particles in turbulence: II. Comparing simulation with experiment, New Journal of Physics, 14, 10.1088/1367-2630/14/10/105031, 2012.

Shaw, R. A., Kostinski, A. B., and Larsen, M. L.: Towards quantifying droplet clustering in clouds, Quarterly Journal of the Royal Meteorological Society, 128, 1043-1057, 10.1256/003590002320373193, 2006.

Shupe, M. D., Zuidema, P., Morrison, H., Mrowiec, A., Avramov, A., Ackerman, A. S., van Diedenhoven, B., and Fridlind, A. M.: A FIRE-ACE/SHEBA Case Study of Mixed-Phase Arctic Boundary Layer Clouds: Entrainment Rate Limitations on Rapid Primary Ice Nucleation Processes, J. Atmos. Sci., 69, 365-389, 10.1175/jas-d-11-052.1, 2012.

Taylor, P. C., Boeke, R. C., Li, Y., Thompson, D. W. J. A. C., and Physics: Arctic cloud annual cycle biases in climate models, 19, 8759-8782, 2019.

Wang, A., Krueger, S., Chen, S., Ovchinnikov, M., Cantrell, W., and Shaw, R. A.: Glaciation of Mixed-Phase Clouds: Insights from Bulk Model and Bin-Microphysics Large-Eddy Simulation Informed by Laboratory Experiment, 10.5194/egusphere-2024-1140, 2024.

Wang, Y., Kong, R., Cai, M., Zhou, Y., Song, C., Liu, S., Li, Q., Chen, H., and Zhao, C.: High small ice concentration in stratiform clouds over Eastern China based on aircraft observations: Habit properties and potential roles of secondary ice production, Atmospheric Research, 281, 10.1016/j.atmosres.2022.106495, 2023.

Wegener, A.: Thermodynamik der Atmosphäre, J. A. Barth, 393, 1911.

Whittaker, R. H.: Evolution and measurement of species diversity, YTAXON, 21, 213-251, 1972.

Yang, J., Lu, J., Deng, Y., Wang, Y., Lu, C., Yin, Y., Wang, Z., Jing, X., and Yang, K.: Parameterizing the Heterogeneous Liquid-Ice Mixing in Modeling Ice Growth Through the Wegener-Bergeron-Findeisen Process in CAM6, Geophysical Research Letters, 52, 10.1029/2024gl114036, 2025.

https://doi.org/10.5194/egusphere-2026-5798
Preprint. Discussion started: 13 November 2026
© Author(s) 2026. CC BY 4.0 License.



Yang, J., Qin, Z., Deng, Y., Chen, M., Jing, X., Yin, Y., Lu, C., Chen, B., Zhang, B., and Bao, X.: On the Cluster Scales of Hydrometeors in Mixed-Phase Stratiform Clouds, Geophysical Research Letters, 51, 10.1029/2024gl108166, 2024.

Zelinka, M. D., Myers, T. A., McCoy, D. T., Po-Chedley, S., Caldwell, P. M., Ceppi, P., Klein, S. A., and Taylor, K. E.: Causes of higher climate sensitivity in CMIP6 models, Geophysical Research Letters, 47, e2019GL085782, 2020.

Zhang, T., Li, L., Liu, Y., ́opez-Marrero, V. L., Yang, F., Atif, M., Ladeinde, F., Sharfuddin, A. A. M., and Lin, M.: Emulator of PR-DNS: Part II, Accelerating thermodynamics and cloud droplet fields with machine learning in Particle-Resolved Direct Numerical Simulation, Journal of Advances in Modeling Earth Systems, 10.22541/essoar.172858028.85856778/v1, 2024.